

# An unsupervised deep learning approach in solving partial-integro differential equations

Weilong Fu\* Ali Hirsal†

## Abstract

We investigate solving partial integro-differential equations (PIDEs) using unsupervised deep learning in this paper. To price options, assuming underlying processes follow Lévy processes, we require to solve PIDEs. In supervised deep learning, pre-calculated labels are used to train neural networks to fit the solution of the PIDE. In an unsupervised deep learning, neural networks are employed as the solution, and the derivatives and the integrals in the PIDE are calculated based on the neural network. By matching the PIDE and its boundary conditions, the neural network gives an accurate solution of the PIDE. Once trained, it would be fast for calculating options values as well as option Greeks.

**Keywords:** PIDEs, neural networks, deep learning

## 1 Introduction

Financial models based on Lévy processes are better at describing the fat tails of asset returns and matching the implied volatility surfaces in option markets than the diffusion models, since Lévy processes take jumps into consideration in addition to Gaussian movements. Some examples of the models are the variance gamma model (VG, [16]), the normal inverse gamma model (NIG, [1]), and the tempered stable process (also known as the CGMY model, [2]).

The partial integro-differential equation (PIDE) is used to calculate the option values for the models based on Lévy processes. Its difference from the partial differential equation (PDE) for the diffusion models is the integral term, which is due to jumps in Lévy processes. For this reason, the PIDE is harder to solve and subsequently options under Lévy processes are more complex to price. The PIDE can be solved utilizing the finite difference method in an explicit-implicit scheme as described in [9], or the fast Fourier transform (FFT) (see [3] and [15] for details).

Recently, many pricing approaches are proposed based on machine learning (ML) and deep learning (DL).

- In [4], kernel regression is applied to the pre-calculated data to price American options. The PIDE is converted into an ordinary integro-differential equation (OIDE) and kernel regression is used to calculate a correction term in the OIDE to reduce the error.
- In supervised deep learning, a priori, many labels are generated by other pricing methods. Then neural networks are employed to fit the price surface or the volatility surface as a function w.r.t. all the parameters involved in the model (see e.g. [8],[14],[11]). The advantage of neural network approaches is that they are fast in

---

\*Department of IEOR, Columbia University, wf2232@columbia.edu

†Department of IEOR, Columbia University, ah2347@columbia.edu

computing prices once trained. However, in supervised learning, it is pretty costly to generate the training labels.

- There are unsupervised learning approaches as well. In [17], the authors consider the problem of solving a PDE by neural networks. The derivatives in the PDE are calculated from the neural network and they try to match the two sides of the PDE and its boundary conditions. In this way, the solution of the PDE is solved and no labels is needed for training the neural network.

In [17], only a PDE is considered, and we aim to extend the approach to the PIDE. In this paper, we solve the PIDE by neural network directly. The neural network only needs to be trained once, which is the same as supervised deep learning. The main difference from supervised deep learning is that this approach is a self-contained pricing one, which does not need pre-calculated labels.

The paper is organized as follows. In Section 2, we describe the problem of solving the PIDE. The variance gamma model is used as an example. In Section 3, we explain how to calculate derivatives and integrals. In Section 4, we testify the unsupervised deep learning approach in pricing options. Many choices of the neural network parameters are implemented to compare the performance. Also, the same method is applied to the Black-Merton-Scholes model to show the effect of the integral in the PIDE. At last, we show the outcome for option Greeks. Section 5 summarizes the paper.

## 2 Problem

### 2.1 Model

In this paper, we choose the variance gamma (VG) model ([16]) as an example. It is a pure jump process with three model parameters  $\theta$ ,  $\sigma$  and  $\nu$ . The Lévy density of the VG process is given by

$$k(x) = \frac{e^{-\lambda_p x}}{\nu x} 1_{x>0} + \frac{e^{-\lambda_n |x|}}{\nu |x|} 1_{x<0}, \quad (1)$$

where

$$\lambda_p = \left( \frac{\theta^2}{\sigma^4} + \frac{2}{\sigma^2 \nu} \right)^{\frac{1}{2}} - \frac{\theta}{\sigma^2}$$

and

$$\lambda_n = \left( \frac{\theta^2}{\sigma^4} + \frac{2}{\sigma^2 \nu} \right)^{\frac{1}{2}} + \frac{\theta}{\sigma^2}.$$

### 2.2 PIDE

Suppose  $S$  is the stock price,  $K$  is the strike price,  $T$  is the maturity,  $r$  is the risk-free interest rate and  $q$  is the dividend rate. In the VG model, the price of the European options can be solved through the following PIDE

$$\begin{aligned} \int_{-\infty}^{\infty} \left[ V(Se^x, t) - V(S, t) - \frac{\partial V}{\partial S}(S, t) S(e^x - 1) \right] k(x) dx \\ + \frac{\partial V}{\partial t}(S, t) + (r - q) S \frac{\partial V}{\partial S}(S, t) - rV(S, t) = 0. \end{aligned} \quad (2)$$

with the initial condition  $V(S, T) = (K - S)^+$  for put options or  $V(S, T) = (S - K)^+$  for call options. Here  $V(S, t)$  is the price and  $k(x)$  is the Lévy density as given in (1).

By making change of variables,  $x = \ln S$ ,  $\tau = T - t$ , and  $w(x, \tau) = V(S, t)$ , we get

$$\begin{aligned}\frac{\partial w}{\partial x}(x, \tau) &= S \frac{\partial V}{\partial S}(S, t), \\ \frac{\partial w}{\partial \tau}(x, \tau) &= -\frac{\partial V}{\partial t}(S, t), \\ w(x + y, \tau) &= V(Se^y, t),\end{aligned}$$

and the following equation

$$\begin{aligned}\int_{-\infty}^{\infty} \left[ w(x + y, \tau) - w(x, \tau) - \frac{\partial w}{\partial x}(x, \tau)(e^y - 1) \right] k(y) dy \\ - \frac{\partial w}{\partial \tau}(x, \tau) + (r - q) \frac{\partial w}{\partial x}(x, \tau) - rw(x, \tau) = 0.\end{aligned}\quad (3)$$

with the initial condition  $w(x, 0) = (K - e^x)^+$  for put options or  $w(x, 0) = (e^x - K)^+$  for call options. Here  $x = \log(S)$  is the log-price and  $\tau$  is the time to maturity.

Our goal is to solve the PIDE in (3) utilizing neural networks directly. We treat the solution  $w(\cdot)$  as a function of  $x$  and  $\tau$  as well as other parameters, substitute  $w(\cdot)$  with a multi-layer perceptron and train the network to satisfy the PIDE. This is an unsupervised method which means there is no need for labels which are option prices calculated by other methods. For this study we just focus on the European put.

### 3 Calculation

#### 3.1 Derivatives and integral

In the neural network, we always use a smooth activation function to build the solution  $w(x, \tau)$ , e.g., swish ( $f(x) = x \sigma(x)$ , where  $\sigma(\cdot)$  is the sigmoid function) or softplus ( $f(x) = \ln(e^x + 1)$ ). Thus the derivatives  $\frac{\partial w}{\partial x}(x, \tau)$  and  $\frac{\partial w}{\partial \tau}(x, \tau)$  are calculated by backward propagation. Given a point  $(x, \tau, \Theta)$ , where  $\Theta = \{\sigma, \nu, \theta, r, q\}$ , we calculate the integral

$$\int_{-\infty}^{\infty} \left[ w(x + y, \tau) - w(x, \tau) - \frac{\partial w}{\partial x}(x, \tau)(e^y - 1) \right] k(y) dy$$

in two parts. The inner part

$$\int_{|y| < \epsilon} \left[ w(x + y, \tau) - w(x, \tau) - \frac{\partial w}{\partial x}(x, \tau)(e^y - 1) \right] k(y) dy$$

is approximated by

$$\left[ \frac{\partial^2 w}{\partial x^2}(x, \tau) - \frac{\partial w}{\partial x}(x, \tau) \right] \int_{|y| \leq \epsilon} \frac{y^2}{2} k(y) dy$$

the same way as described in Chapter 5 in [7]. For the outer part, we can write

$$\begin{aligned}\int_{|y| > \epsilon} \left[ w(x + y, \tau) - w(x, \tau) - \frac{\partial w}{\partial x}(x, \tau)(e^y - 1) \right] k(y) dy \\ = \int_{|y| > \epsilon} [w(x + y, \tau) - w(x, \tau)] k(y) dy - \frac{\partial w}{\partial x}(x, \tau) \int_{|y| > \epsilon} (e^y - 1) k(y) dy\end{aligned}$$

The first portion of it is calculated using the trapezoidal rule as explained in [21]. Further details are included in Appendix A.

### 3.2 Loss function

The Cauchy boundary conditions are considered:

$$w(x, 0) = (K - e^x)^+ \quad (4)$$

$$w(x_{min}, \tau) = Ke^{-r\tau} - e^{x_{min}-q\tau} \quad (5)$$

$$w(x_{max}, \tau) = 0 \quad (6)$$

Given a sample point  $(x, \tau, \Theta)$ , the loss function is the sum of the squared differences of the residuals in Equations (3), (4), (5) and (6).

## 4 Numerical experiments

### 4.1 Input dimension

For the VG model, the input dimension of the neural network is seven in total, which are  $x, \tau, r, q, \theta, \sigma$  and  $\nu$ . In other models based on Lévy processes, there would be more or fewer parameters and the input dimension of the neural network should vary accordingly. The input dimension does not influence the outcome since the input dimension is small compared with the dimension of neurons.

### 4.2 Variants of the neural networks

We consider networks consisting of  $1 \leq L \leq 6$  layers, with  $n \in \{100, 200, 300, 400, 500, 600\}$  neurons in each layer. The activation is chosen from swish and softplus. Initialization changes among he-normal, he-uniform [6], lecun-normal, lecun-uniform [13], glorot-normal and glorot-uniform [5]. The initial distributions are uniform distributions with different ranges or truncated normal distributions with different variances. For example, the he-normal initialization employs a truncated normal distribution with the variance  $2/N_{in}$  where  $N_{in}$  is the input size of the layer. The optimizer could be Adam [12] or RMSprop [20]. We also consider regularization of batch-normalization [10] and different dropout rates [19]. We then try different boundary conditions and assess the performance of the integral. Finally, we test the effect of the sample size.

### 4.3 Settings of parameters

We consider the option price  $w(\cdot)$  in the following region:

$$\begin{aligned} 0 < \tau &\leq 3, \\ 1\% \leq \sigma &\leq 50\%, \\ 0.1 \leq \nu &\leq 0.6, \\ -0.5 \leq \theta &\leq -0.1, \\ 0 \leq r, q &\leq 0.1 \end{aligned}$$

The strike  $K$  is fixed to 200. We use  $\epsilon = 0.01$  for the integral calculation. For the boundary conditions, we assume  $x_{min} = \ln(1)$  and  $x_{max} = \ln(10000)$ . For the training samples, the log-price  $x$  follows the uniform distribution between  $\ln(K/40)$  and  $\ln(2K)$ . For the test samples, the log-price  $x$  follows the uniform distribution between  $\ln(K/2)$  and  $\ln(2K)$ . The log-price  $x$  of the test samples are restricted between  $\ln(K/2)$  and  $\ln(2K)$  since we do not want to focus too much on the deep in-the-money options. The other parameters are uniformly distributed within their ranges.

Here we start from a training size of 50000 and a test size of 2000. The batch size is 200 and the training epochs is 30 and they will be the same in the following experiments

unless specified otherwise. The samples are given by the Sobol sequence ([18]), which is a quasi random sequence.

#### 4.4 Initialization

Given  $L = 3$  layers and  $N = 200$  neurons in each layer, we test different initializations. The activation is swish and the optimizer is Adam. No regularization is used. As shown in Table 1, he-normal initialization gives the best outcome, and we choose he-normal going forward in our study.

#### 4.5 Activation

We compare swish and softplus, with the optimizer Adam and no regularization. As shown in Table 2, swish performs uniformly better than softplus. We will continue with swish in the following part.

#### 4.6 Optimizer

We compare Adam and RMSprop without any regularization. As shown in Table 3, Adam performs uniformly better than RMSprop. We will continue with swish in the following part.

#### 4.7 Batch normalization

We now test batch-normalization. As shown in Table 4, there is no obvious improvement with batch-normalization. Considering batch normalization is costly, we prefer not to use it.

#### 4.8 Number of layers and size of each layer

We now test the number of layers  $L$  and neuron size  $N$  in each layer. The best combinations are  $(L, N) = (4, 600)$ ,  $(L, N) = (5, 400)$  and  $(L, N) = (5, 500)$  as shown in Table 5. We would choose  $4 \leq L \leq 5$  and  $400 \leq N \leq 600$ .

#### 4.9 Dropout

When we choose  $L = 4$  and  $N = 400$ , the best choice for the dropout rate is 0.3. However, if we choose  $L = 4$  and  $N = 200$ , the best choice for the dropout rate seems to be 0.2. So the optimal dropout rate choice depends on the size of the network and cannot be fixed.

Also, a dropout rate slightly larger than 0 does not always reduce the error. We can easily see this phenomenon in Table 7. The best performance is reached at a very large dropout rate. There are cases that dropout does not help at all, as can be seen in Tables 12 and 14. Typically, for certain neural networks, we try different dropout rates and pick the best one.

#### 4.10 Boundary conditions

We illustrate in Table 8 the result of replacing Dirichlet boundary conditions

$$\begin{aligned} w(x_{min}, \tau) &= Ke^{-r\tau} - e^{x_{min}-q\tau} \\ w(x_{max}, \tau) &= 0 \end{aligned}$$

	RMSE	MAE
glorot-normal	2.434	13.266
glorot-uniform	2.125	10.107
<b>he-normal</b>	<b>1.954</b>	<b>10.140</b>
he-uniform	2.090	10.106
lecun-normal	1.956	10.433
lecun-uniform	2.129	11.486

Table 1: Root mean squared error (RMSE) and maximum absolute error (MAE).

	RMSE	
	softplus	swish
$L = 3, N = 100$	2.808	2.468
$L = 3, N = 200$	2.309	1.954
$L = 3, N = 300$	1.861	1.614
$L = 3, N = 400$	1.845	1.733

Table 2: Root mean squared error (RMSE).

	Adam		RMSprop	
	RMSE	MAE	RMSE	MAE
$L = 3, N = 100$	2.468	11.586	4.333	14.905
$L = 3, N = 200$	1.954	10.140	3.033	13.991
$L = 3, N = 300$	1.614	8.569	3.075	9.670
$L = 3, N = 400$	1.733	10.668	2.170	10.345

Table 3: Root mean squared error (RMSE) and maximum absolute error (MAE).

	False		True	
	RMSE	MAE	RMSE	MAE
$L = 3, N = 100$	2.468	11.586	2.135	10.366
$L = 3, N = 200$	1.954	10.140	2.294	12.299
$L = 3, N = 300$	1.614	8.569	1.888	9.882
$L = 3, N = 400$	1.733	10.668	1.604	9.183

Table 4: Root mean squared error (RMSE) and maximum absolute error (MAE).

RMSE		N						
		100	200	300	400	500	600	700
L	1	35.942	18.907	17.124	15.574	14.980		
	2	2.744	2.400	2.438	2.458	2.579		
	3	2.468	1.954	1.614	1.733	1.744	1.269	1.502
	4	2.143	1.860	1.657	1.401	1.221	0.981	1.229
	5	1.769	1.285	1.794	1.119	1.033	1.729	1.201
	6	1.706	1.261	1.396	1.708	1.362	1.664	1.167

Table 5: Root mean squared error (RMSE).

with Neumann boundary conditions

$$\begin{aligned}\frac{\partial^2 w}{\partial x^2} w(x_{min}, \tau) - \frac{\partial w}{\partial x} w(x_{min}, \tau) &= 0 \\ \frac{\partial^2 w}{\partial x^2} w(x_{max}, \tau) - \frac{\partial w}{\partial x} w(x_{max}, \tau) &= 0\end{aligned}$$

For small  $N$ , assuming Neumann conditions, the results are generally better when considering the Dirichlet conditions. However, for large  $N$ , the results of the Neumann conditions are worse. Also, as we see from Table 8, the results of the Neumann conditions are less stable and not consistent. There are cases that the results are better and on the other hand there are cases that they are worse.

#### 4.11 Integral grid

In this part we would like to test whether the error of the numerical integral leads to errors in pricing. In Appendix A we explain how to calculate the integral

$$\int_{y>\epsilon} [w(x+y, \tau) - w(x, \tau)] k(y) dy$$

via the trapezoid rule. If we split each integral interval into two halves, i.e., add the mid point of each integral interval to the grid points, then we get a finer grid and can reduce the error of the trapezoid rule. We can compare the performance of the finer grid and the original grid to check if the error of the integral would influence training. When we take the finer grid, the error gets slightly larger. So approximation due to usage of the trapezoid rule is not the reason for the error.

#### 4.12 Fixed integral

In this part we would like to test whether it is stable to update the numerical integral, which involves the output of the neural network at many points. In each step of training, we need to consider the integral as a function of the network parameters and take the derivatives. That is actually pretty time consuming and computationally expensive. If we treat the integral as a constant and do not update the integral in each step, we do not have to take the derivatives of the integral with regard to the network parameters. This is consistent with the explicit-implicit finite difference scheme proposed in [9]. This approach is faster, but the error is still larger than the original method. This is easy to understand since we use integral approximation from the last step in training to approximate the integrals of the current step. Since the fixed integral does not reduce errors, we are not concerned about the stability of the numerical integral.

#### 4.13 Comparison with the Black-Merton-Scholes (BMS) model

To see the impact of the jump integral we consider solving the BMS equation

$$-\frac{\partial w}{\partial \tau}(x, \tau) + \frac{\sigma^2}{2} \frac{\partial^2 w}{\partial x^2}(x, \tau) + \left(r - q - \frac{\sigma^2}{2}\right) \frac{\partial w}{\partial x}(x, \tau) - rw(x, \tau) = 0.$$

The performance is provided in Tables 11 & 12.

Note that there is no integral term in the BMS equation. If the integral term is the main reason for the errors in the VG model, the errors in the BMS model should be much smaller. But in fact, with neural networks of the same size, the errors in the BMS model are just slightly smaller than those in the VG model. Also note that the BMS model is the special case of the VG model when  $\nu = 0$  and  $\theta = 0$ . The dimension of the sample

dropout rate	$L = 4, N = 400$		$L = 4, N = 200$	
	RMSE	MAE	RMSE	MAE
0	1.954	10.140	1.860	6.606
0.1	2.092	7.114	1.708	10.718
0.2	1.201	8.232	1.522	10.250
0.3	0.955	4.764	1.612	10.488
0.4	1.211	6.760	1.635	8.638

Table 6: Root mean squared error (RMSE) and maximum absolute error (MAE).

dropout rate	$L = 4, N = 600$		$L = 5, N = 500$	
	RMSE	MAE	RMSE	MAE
0.0	0.981	6.031	0.864	3.848
0.1	0.752	3.585	1.265	8.555
0.2	1.512	8.228	1.227	5.744
0.3	2.507	10.394	1.335	8.298
0.4	1.009	6.937	1.510	8.554
0.5	1.894	6.381	0.742	3.886
0.6	0.831	6.277	1.248	6.913
0.7	1.387	8.294	1.193	6.990

Table 7: Root mean squared error (RMSE) and maximum absolute error (MAE).

$N$	Neumann		Dirichlet	
	$L = 4$	$L = 5$	$L = 4$	$L = 5$
100	1.941	1.422	2.143	1.769
200	1.254	0.842	1.860	1.285
300	1.512	1.109	1.657	1.794
400	2.823	0.633	1.401	1.119
500	1.675	1.754	1.221	1.033

Table 8: Root mean squared error (RMSE).

$L = 4, N = 400, \text{ dropout}=0.3$	RMSE	MAE
original grid	1.081	6.776
finer grid	1.260	7.662

Table 9: Root mean squared error (RMSE) and maximum absolute error (MAE).

$L = 4, N = 400, \text{ dropout}=0.3$	RMSE	MAE
original method	1.081	6.776
fixed integral	1.249	5.611

Table 10: Root mean squared error (RMSE) and maximum absolute error (MAE).



space in the BMS model is 5, while the dimension in the VG model is 7. The BMS model should be less affected by the curse of dimensionality and we should expect that the errors of neural networks are slightly smaller under the BMS model given the same sample size. From these results we can conclude that the integral part is not the main reason of the error.

#### 4.14 Fully trained networks

The previous tests are to find the suitable neural networks for pricing and test the performance of the boundary conditions and the numerical integral. Then we train the networks on large samples for many epochs to get the full performance. Tables 13-15 contain the outcomes of large samples from 50,000 to 1,000,000. Since the batch size is fixed to 200, there are more timesteps in one epoch if the sample size is larger and more timesteps usually means better results in the optimization algorithms. To be fair in our comparison, we need to keep the total timesteps the same even if the sample sizes are different. This is fair also because the time costs will be the same for different sample sizes. For the size of 50,000, 200,000, 500,000 and 1,000,000, the number of epochs are 600, 150, 60, and 30 respectively. Thus the total timesteps of optimization is

$$\frac{1,000,000}{200} \times 30 = 150,000.$$

The neural networks of the best performance are listed in Table 13. The RMSE is about 0.1, which is quite small. The MAE is about 1, which is 10 times as large as the RMSE, which means the neural network is quite close to the true price surface, but with a few large meanderings.

In Table 14, we show that dropout would not always work. For larger sizes such as  $L = 5, N = 500$  or  $L = 4, N = 600$ , dropout deteriorates performance. But when the size is larger, dropout exacerbates.

In Table 15, we fix the structure of the neural network and just change the sample size. When we increase the sample size from 50,000 to 1,000,000, the performance is about the same.

#### 4.15 Summary of model selection

Until now, we find it is better to use **he-normal** initialization, with swish activation, Adam optimizer and no batch-normalization. A larger network gives better outcomes and the optimal dropout rate should be selected specifically. The Dirichlet boundary conditions and the trapezoid rule work well in the method. The integral term does not increase the error in the approach. The number of total timesteps plays a more important role than the sample size in fully training the neural network.

#### 4.16 Prediction of prices and Greeks

In Figures 1 and 2, we show the curves of the price, Delta, Gamma, and Theta and compare the true values and the predicted values from the neural network. The true value are computed through the fast Fourier transform (FFT).[?] The predicted value is calculated from the neural network by back propagation. Suppose  $V(S, t)$  is the price an option of a certain strike  $K$ . Then Delta is  $\frac{\partial V}{\partial S}$ , Gamma is  $\frac{\partial^2 V}{\partial S^2}$  and Theta is  $\frac{\partial V}{\partial t} = -\frac{\partial V}{\partial \tau}$ . Note that this **Theta** is one of the options Greeks and is different from the model parameter  $\theta$  in the VG model. The model for prediction is the network of  $L = 5, N = 500$  and dropout=0 in Section 4.14 after 30 epochs of training.

In Figure 1, we choose  $K = 200, \tau = 1$  (1 year),  $r = 0.05, q = 0.02, \theta = -0.4, \sigma = 0.4$  and  $\nu = 0.4$ . In Figure 2, all the parameters are the same except  $\tau = 3$  (3 years). Even

RMSE		N			
		300	400	500	600
L	4	1.101	0.774	1.412	0.981
	5	0.955	1.100	0.684	0.882

Table 11: Root mean squared error (RMSE).

$L = 5, N = 500$		
dropout rate	RMSE	MAE
0.0	0.684	3.659
0.1	3.721	10.742
0.2	1.244	6.841
0.3	1.942	6.482
0.4	0.960	4.942
0.5	0.973	4.669

Table 12: Root mean squared error (RMSE) and maximum absolute error (MAE).

size = 1000000	RMSE	MAE
$L = 5, N = 500, \text{ dropout}=0$	0.113	0.976
$L = 4, N = 400, \text{ dropout}=0.3$	0.128	1.161
$L = 4, N = 600, \text{ dropout}=0$	0.173	1.451

Table 13: Root mean squared error (RMSE) and maximum absolute error (MAE).

size = 1000000	RMSE	MAE
$L = 5, N = 500, \text{ dropout}=0$	0.113	0.976
$L = 5, N = 500, \text{ dropout}=0.3$	0.179	1.248
$L = 5, N = 500, \text{ dropout}=0.5$	0.226	1.417

Table 14: Root mean squared error (RMSE) and maximum absolute error (MAE).

$L = 5, N = 500, \text{ dropout}=0$	RMSE	MAE
size = 50000	0.111	1.136
size = 200000	0.125	0.970
size = 500000	0.142	1.163
size = 1000000	0.113	0.976

Table 15: Root mean squared error (RMSE) and maximum absolute error (MAE).

though we only want to fit an approximate solution of the price, we also get the option Greeks from the neural network. Here we only show the option Greeks w.r.t. price and time. In fact, we can get the Greeks w.r.t.  $r$ ,  $q$  and all the model parameters from the neural network by back propagation.

## 5 Conclusion

In this paper we have proposed a pricing approach using unsupervised deep learning. Especially, we use neural networks to express the solutions and solve the PIDE for models based on Lévy processes. The first benefit of this approach is that we only need to train the neural network once for a certain model. The second benefit is that we do not need labels for training. After model selection for neural networks, we find that `he-normal` initialization, swish activation, Adam optimizer and no batch-normalization perform well in this approach. We analyze that the integral term in the PIDE does not influence option and option Greeks approximation in the approach and the error of prediction shrinks after more training epochs. Also, the approach does not only give the option price itself, but also the option Greeks.

We only study the European options in the paper. For future study, it is attractive to extend the same approach to price American options under Lévy processes.

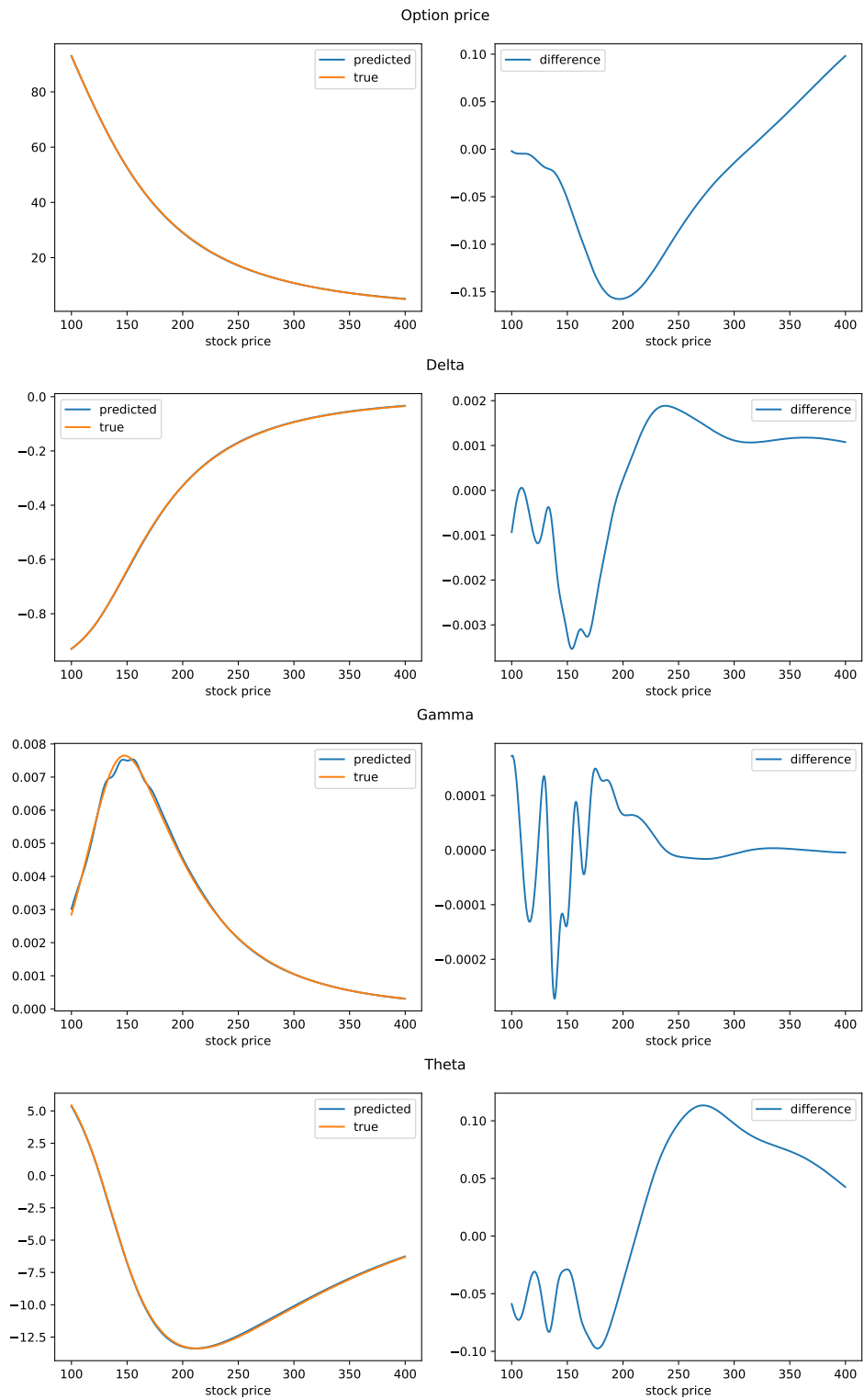


Figure 1: Price, Delta, Gamma and Theta when  $\tau = 1$ ,  $r = 0.05$ ,  $q = 0.02$ ,  $\theta = -0.4$ ,  $\sigma = 0.4$  and  $\nu = 0.4$ .

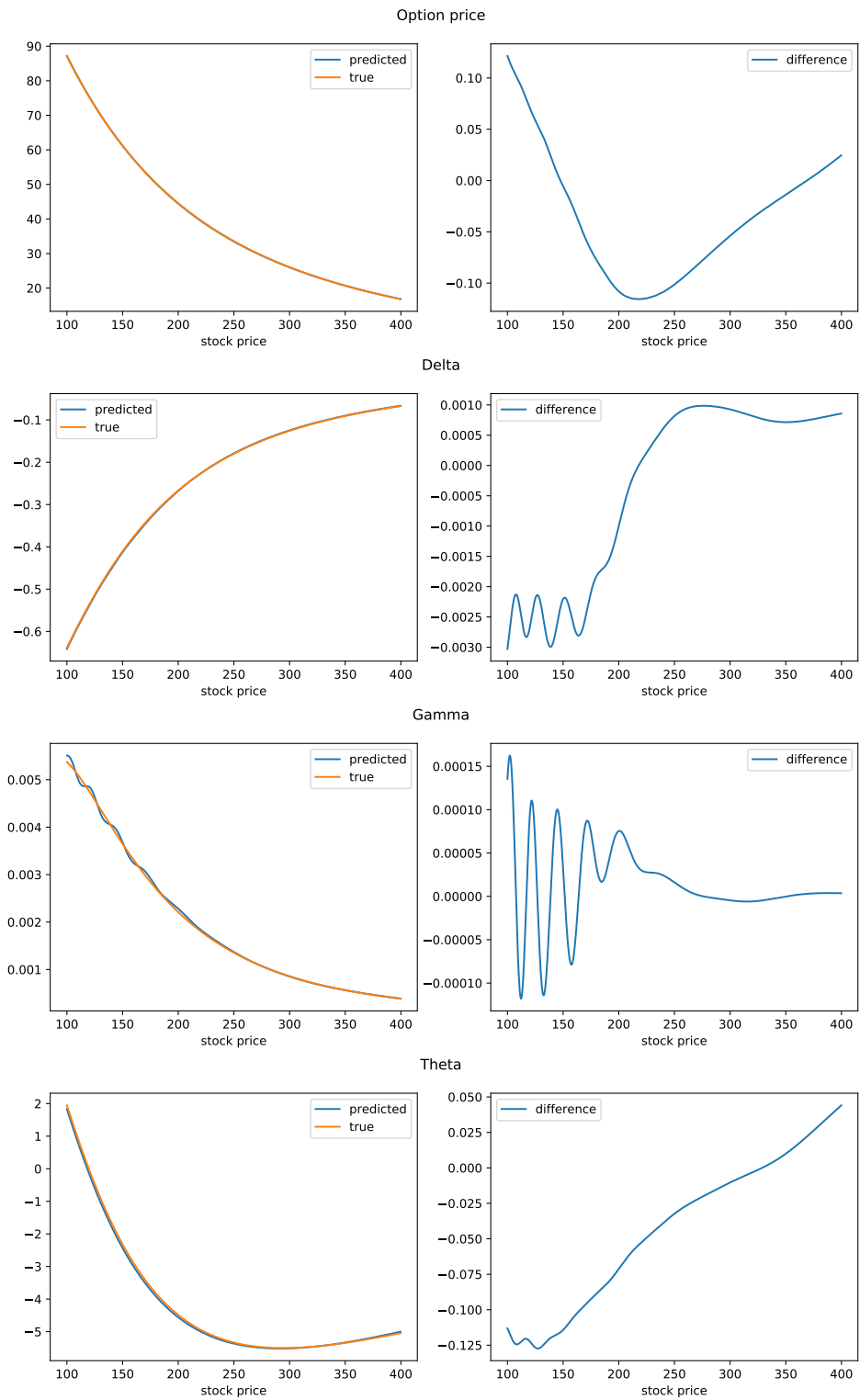


Figure 2: Price, Delta, Gamma and Theta when  $\tau = 3$ ,  $r = 0.05$ ,  $q = 0.02$ ,  $\theta = -0.4$ ,  $\sigma = 0.4$  and  $\nu = 0.4$ .

## References

- [1] O. E. Barndorff-Nielsen. Processes of normal inverse Gaussian type. *Finance and stochastics*, 2(1):41–68, 1997.
- [2] P. Carr, H. Geman, D. B. Madan, and M. Yor. The fine structure of asset returns: An empirical investigation. *The Journal of Business*, 75(2):305–333, Apr. 2002.
- [3] P. Carr and D. Madan. Option valuation using the fast Fourier transform. *The Journal of Computational Finance*, 2(4):61–73, 1999.
- [4] W. Fu and A. Hirsu. A fast method for pricing american options under the variance gamma model, 2019.
- [5] X. Glorot and Y. Bengio. Understanding the difficulty of training deep feedforward neural networks. In *Proceedings of the thirteenth international conference on artificial intelligence and statistics*, pages 249–256, 2010.
- [6] K. He, X. Zhang, S. Ren, and J. Sun. Delving deep into rectifiers: Surpassing human-level performance on imagenet classification, 2015.
- [7] A. Hirsu. *Computational Methods in Finance*. CRC Press, apr 2016.
- [8] A. Hirsu, T. Karatas, and A. Oskoui. Supervised deep neural networks (DNNs) for pricing/calibration of vanilla/exotic options under various different processes. 2019.
- [9] A. Hirsu and D. B. Madan. Pricing American options under variance gamma. *Journal of Computational Finance*, 7(2):63–80, 2003.
- [10] S. Ioffe and C. Szegedy. Batch normalization: Accelerating deep network training by reducing internal covariate shift. In *Proceedings of the 32nd International Conference on International Conference on Machine Learning - Volume 37, ICML’15*, page 448–456. JMLR.org, 2015.
- [11] A. Itkin. Deep learning calibration of option pricing models: some pitfalls and solutions. 2019.
- [12] D. P. Kingma and J. Ba. Adam: A method for stochastic optimization. *arXiv preprint arXiv:1412.6980*, 2014.
- [13] Y. A. LeCun, L. Bottou, G. B. Orr, and K.-R. Müller. Efficient backprop. In *Neural networks: Tricks of the trade*, pages 9–48. Springer, 2012.
- [14] S. Liu, A. Borovykh, L. A. Grzelak, and C. W. Oosterlee. A neural network-based framework for financial model calibration. *Journal of Mathematics in Industry*, 9(1):9, Dec. 2019.
- [15] R. Lord, F. Fang, F. Bervoets, and C. W. Oosterlee. A fast and accurate FFT-based method for pricing early-exercise options under Lévy processes. *SSRN Electronic Journal*, 2007.
- [16] D. B. Madan and E. Seneta. The variance gamma (V.G.) model for share market returns. *The Journal of Business*, 63(4):511, Jan. 1990.
- [17] J. Sirignano and K. Spiliopoulos. Dgm: A deep learning algorithm for solving partial differential equations. *Journal of Computational Physics*, 375:1339 – 1364, 2018.

- [18] I. M. Sobol'. On the distribution of points in a cube and the approximate evaluation of integrals. *Zhurnal Vychislitel'noi Matematiki i Matematicheskoi Fiziki*, 7(4):784–802, 1967.
- [19] N. Srivastava, G. Hinton, A. Krizhevsky, I. Sutskever, and R. Salakhutdinov. Dropout: a simple way to prevent neural networks from overfitting. *The journal of machine learning research*, 15(1):1929–1958, 2014.
- [20] T. Tieleman and G. Hinton. Lecture 6.5-rmsprop: Divide the gradient by a running average of its recent magnitude. *COURSERA: Neural networks for machine learning*, 4(2):26–31, 2012.
- [21] Wikipedia. Trapezoidal rule, [https://en.wikipedia.org/wiki/trapezoidal\\_rule](https://en.wikipedia.org/wiki/trapezoidal_rule).

## Appendices

### A Calculation of the integral

This part follows Chapter 5 in [7]. We can split the integral term in Equation (3) into two terms, the integrals on  $|y| \leq \epsilon$  and  $|y| > \epsilon$  respectively.

In the region  $|y| \leq \epsilon$ ,

$$w(x + y, \tau) = w(x, \tau) + y \frac{\partial w}{\partial x}(x, \tau) + \frac{y^2}{2} \frac{\partial^2 w}{\partial x^2}(x, \tau) + O(y^3)$$

and

$$e^y = 1 + y + \frac{y^2}{2} + O(y^3).$$

Using those two approximations, we get

$$\begin{aligned} & \int_{|y| \leq \epsilon} \left[ w(x + y, \tau) - w(x, \tau) - \frac{\partial w}{\partial x}(x, \tau)(e^y - 1) \right] k(y) dy \\ &= \int_{|y| \leq \epsilon} \left[ \frac{y^2}{2} \frac{\partial^2 w}{\partial x^2}(x, \tau) - \frac{y^2}{2} \frac{\partial w}{\partial x}(x, \tau) + O(y^3) \right] k(y) dy \\ &\approx \int_{|y| \leq \epsilon} \left[ \frac{y^2}{2} \frac{\partial^2 w}{\partial x^2}(x, \tau) - \frac{y^2}{2} \frac{\partial w}{\partial x}(x, \tau) \right] k(y) dy. \end{aligned}$$

Define  $\sigma^2(\epsilon) = \int_{|y| \leq \epsilon} y^2 k(y) dy$  and we get

$$\int_{|y| \leq \epsilon} \left[ w(x + y, \tau) - w(x, \tau) - \frac{\partial w}{\partial x}(x, \tau)(e^y - 1) \right] k(y) dy \approx \frac{1}{2} \sigma^2(\epsilon) \left( \frac{\partial^2 w}{\partial x^2}(x, \tau) - \frac{\partial w}{\partial x}(x, \tau) \right).$$

In the region  $|y| > \epsilon$ ,

$$\begin{aligned} & \int_{|y| > \epsilon} \left[ w(x + y, \tau) - w(x, \tau) - \frac{\partial w}{\partial x}(x, \tau)(e^y - 1) \right] k(y) dy \\ &= \int_{|y| > \epsilon} [w(x + y, \tau) - w(x, \tau)] k(y) dy + \frac{\partial w}{\partial x}(x, \tau) \omega(\epsilon), \end{aligned}$$

where  $w(\epsilon) = \int_{|y| > \epsilon} (1 - e^y) k(y) dy$ .

Combine the two parts of integrals and put them back to Equation (3), and we get

$$\begin{aligned} & \frac{1}{2} \sigma^2(\epsilon) \frac{\partial^2 w}{\partial x^2}(x, \tau) + \int_{|y| > \epsilon} [w(x + y, \tau) - w(x, \tau)] k(y) dy \\ & - \frac{\partial w}{\partial \tau}(x, \tau) + (r - q + \omega(\epsilon) - \frac{1}{2} \sigma^2(\epsilon)) \frac{\partial w}{\partial x}(x, \tau) - r w(x, \tau) = 0. \end{aligned} \quad (7)$$

The derivative terms can be calculated by back-propagation in neural networks. The integral  $\int_{|y| > \epsilon} [w(x + y, \tau) - w(x, \tau)] k(y) dy$  is calculated using the trapezoidal rule. If we let  $\epsilon = 0.01$ , the integrand is calculated over the grid points

$$\{\pm 0.01k : 1 \leq k < 50\} \cup \{\pm 0.05k : 10 \leq k < 20\} \cup \{\pm 0.2k : 5 \leq k < 20\}.$$

Then the trapezoidal rule is applied to approximate the integral over each interval between the grid points. The grid points are denser around 0 and coarser far from 0 because  $w(x + y, \tau)$  is bounded and  $k(y)$  decreases exponentially when  $|y|$  goes to infinity.